Supplementary Information

Soluble Carbon Nitride Nanosheets as an Alternate Precursor for Hard-Templated Morphological Control

Jasper Pankratz,[a] Emma Mitchell,[a] and Robert Godin[*a,b,c]

[a]Department of Chemistry, The University of British Columbia, 3247 University Way, Kelowna, BC, V1V 1V7, Canada.

[b]Clean Energy Research Center, University of British Columbia, 2360 East Mall, Vancouver, BC, V6T 1Z3, Canada.

[c]Okanagan Institute for Biodiversity, Resilience, and Ecosystem Services, University of British Columbia, Kelowna, BC, Canada

Corresponding author email:
robert.godin@ubc.ca

Table of Contents

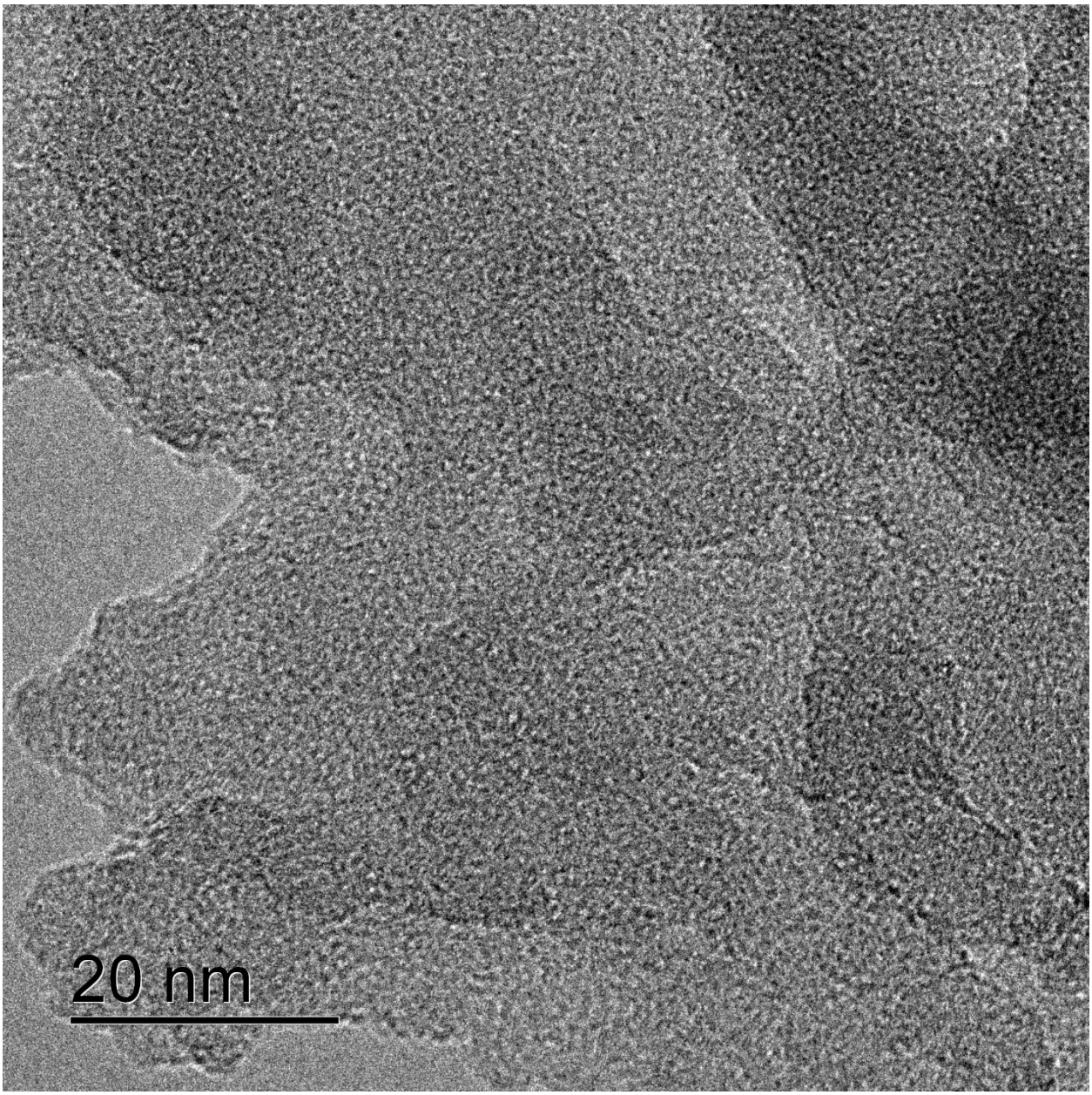

Figure S1. HR-TEM image of sCN_x after etching at 255 kx magnification.

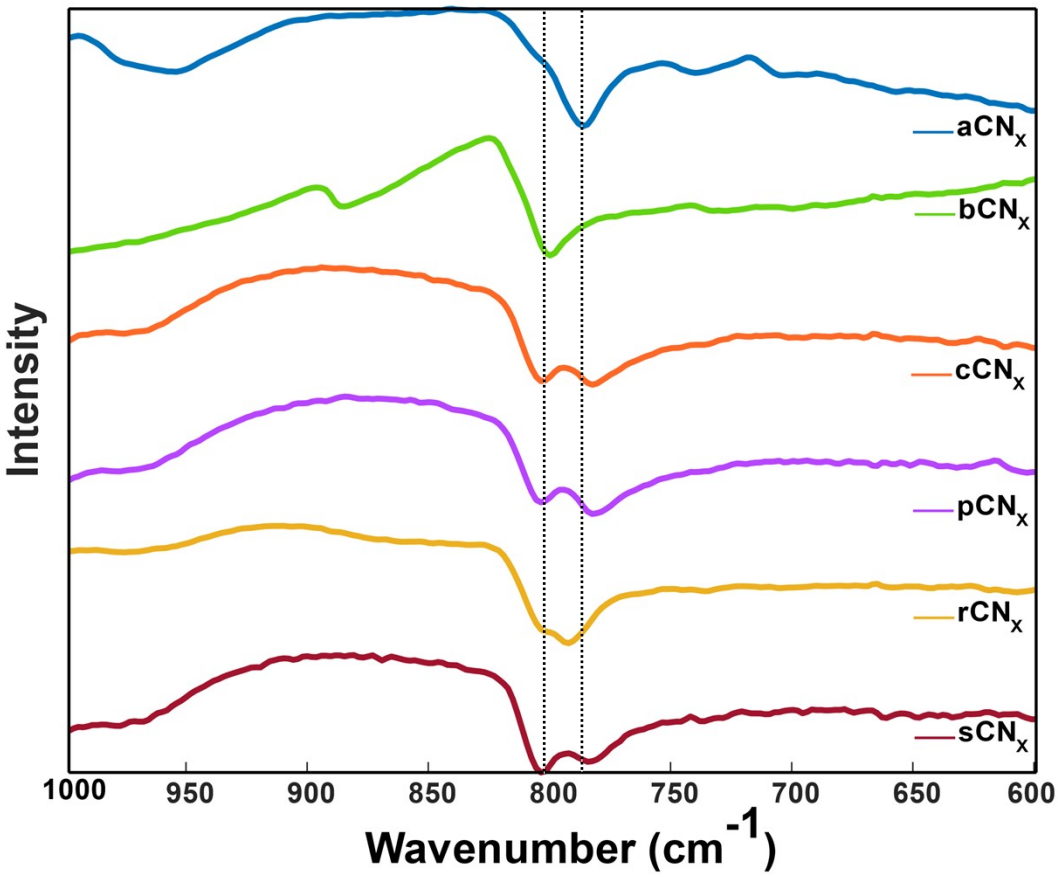

Figure S2. Zoomed in FTIR spectra of the CN_x samples in the region 600 – 1000 cm^{-1}.

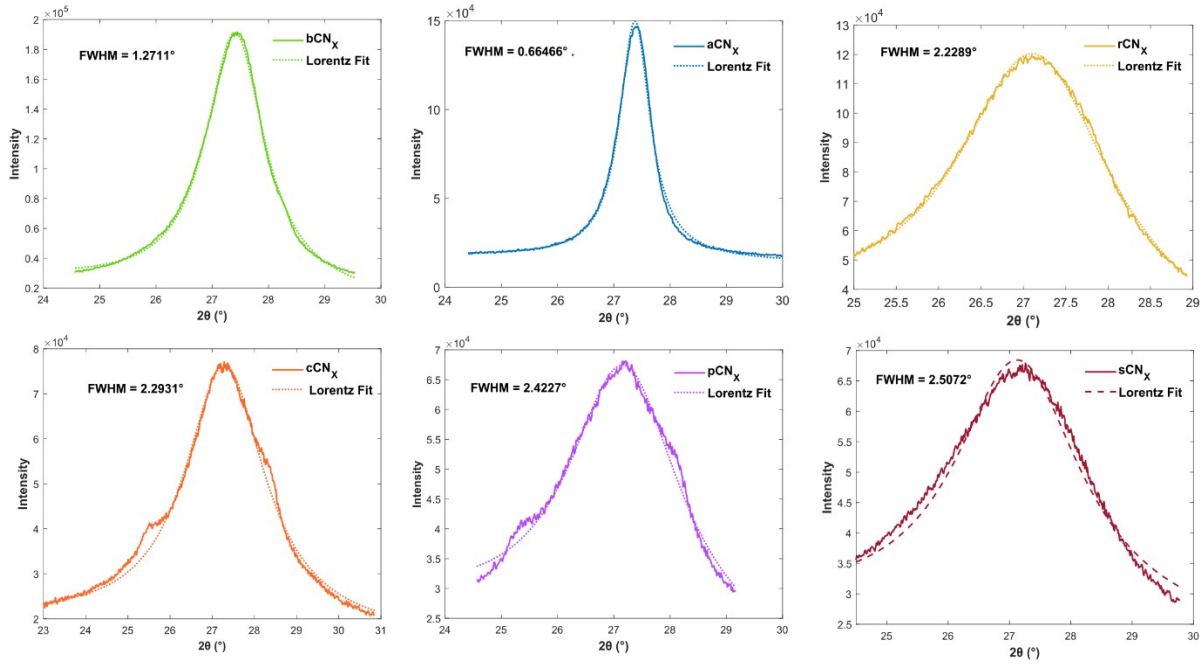

Figure S3. pXRD patterns of the CN_x samples displaying the full width at half maximum (FWHM) values of the (002) peak, determined from a Lorentz fit.

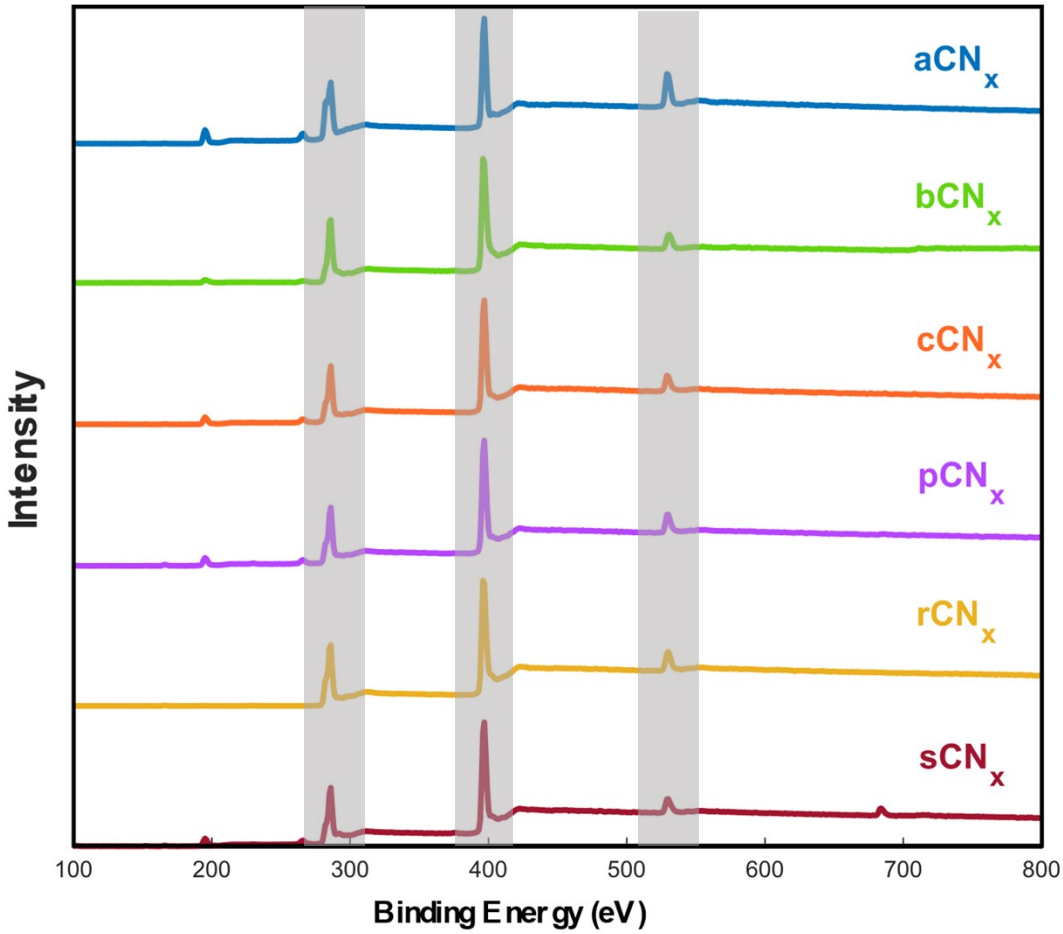

Figure S4. Survey XPS spectra of the CN_x samples. From left to right, the shaded regions correspond to carbon (~ 300 eV), nitrogen (~ 400 eV), and oxygen (~ 530 eV) bonding environments. The small peaks at ~ 200 and 260 eV are from Cl 2p an Cl 2s, respectively and are attributed to the chloride anions of aCN_x and potentially residues from washing the samples with 1M HCl.

Table S1. Relative atomic concentration (%) of C 1s, N 1s, and O 1s peaks in the CN_x samples from the XPS survey scans.

Semiconductor	C1s Atomic Conc (%)	N1s Atomic Conc (%)	O1s Atomic Conc (%)
bCN_X	46.32	44.11	3.94
aCN_X	51.84	37.09	8.27
rCN_X	49.96	44.3	5.60
cCN_X	46.8	46.83	4.57
pCN_X	46.91	45.47	5.51
sCN_X	41.96	48.86	4.79

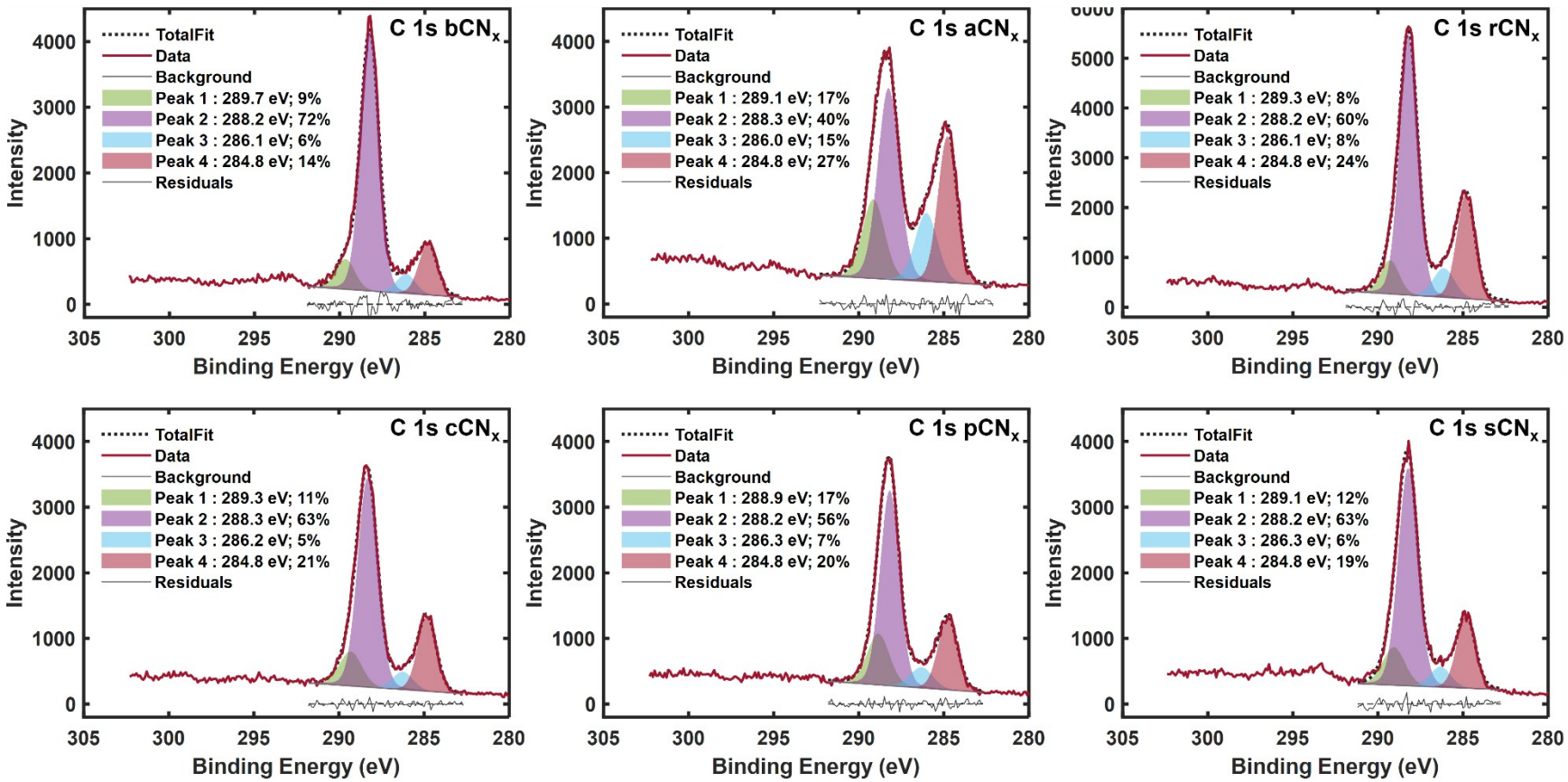

Figure S5. C 1s XPS spectra of the CN_x materials which have been deconvoluted into four main peaks using a linear baseline and Voigt peaks with FWHM of 1.4 eV ± 10%. The Voigt line shape is obtained from a Gaussian-Lorentzian sum with 90% Gaussian character and 10% Lorentzian. The binding energy values have been shifted to the reference value of 284.8 eV for peak 4 corresponding to adventitious C-C environments.

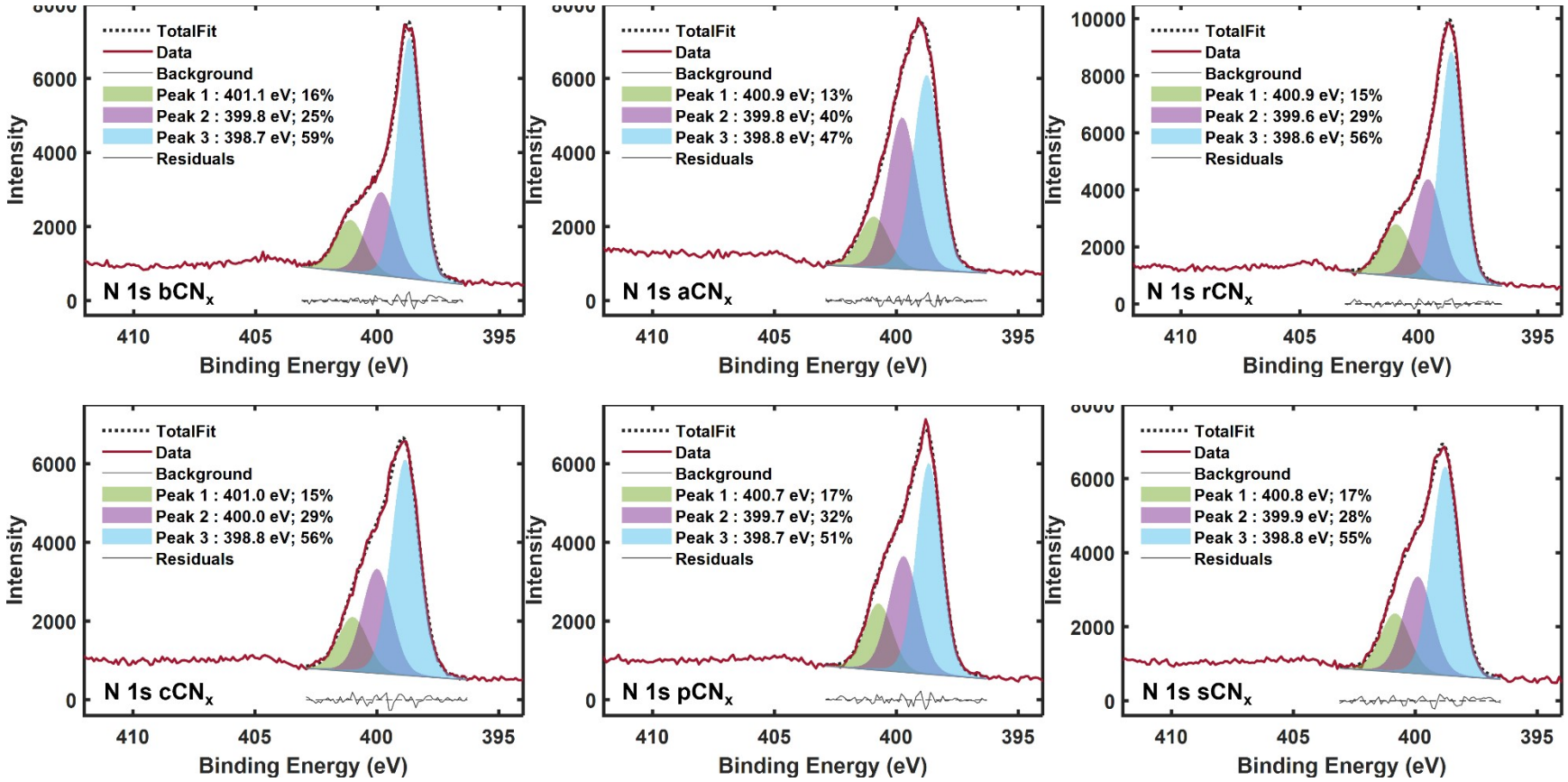

Figure S6. N 1s XPS spectra of the CN_x materials which have been deconvoluted into three main peaks by means of a linear baseline and Voigt peaks with FWHM of 1.3 eV ± 10%. The Voigt line shape is obtained from a Gaussian-Lorentzian sum with 90% Gaussian character and 10% Lorentzian. The binding energy values of each sample have been shifted by the corresponding value of their respective C 1s binding energy shifts.

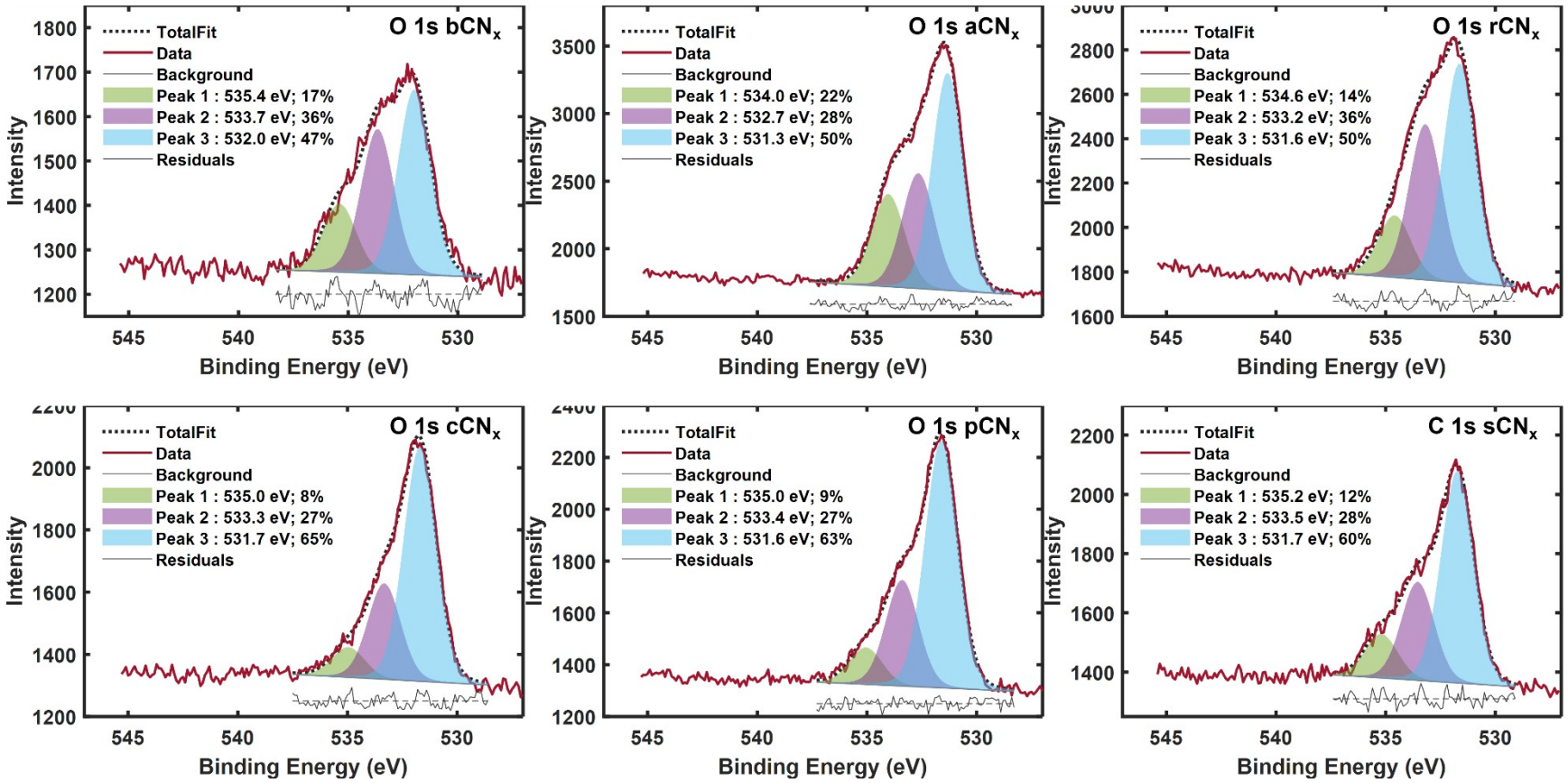

Figure S7. O 1s XPS spectra of the CN_x materials which have been deconvoluted into three main peaks by means of a linear baseline and Voigt peaks with FWHM of 1.6 eV ± 10%. The Voigt line shape is obtained from a Gaussian-Lorentzian sum with 90% Gaussian character and 10% Lorentzian. The binding energy of each sample have been shifted by the corresponding value of their respective C 1s binding energy shifts.

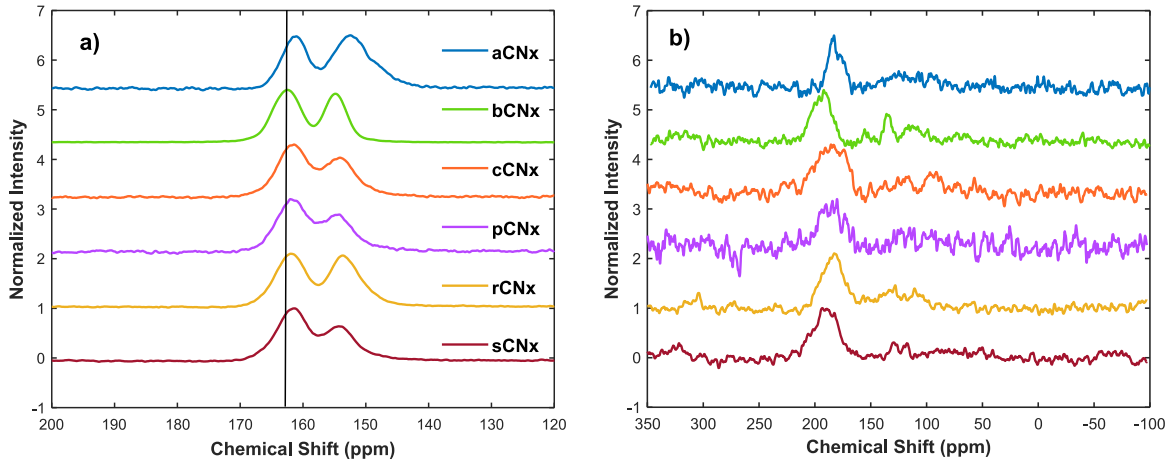

Figure S8. Normalized (a) ^{13}C and (b) ^{15}N solid state NMR spectra for the carbon nitride samples.

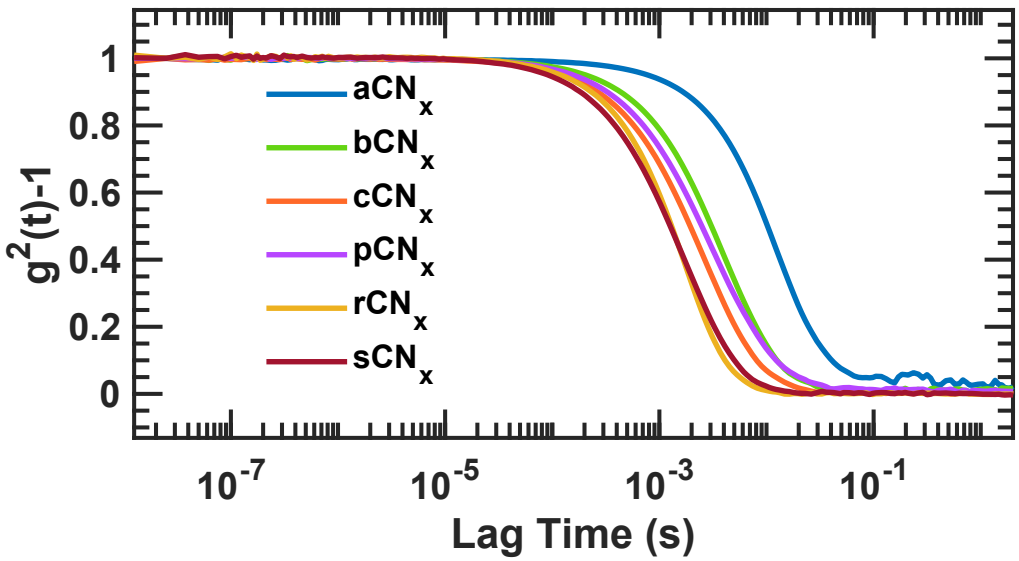

Figure S9. Dynamic light scattering correlation traces acquired in aqueous media at 90° scattering angle. aCN_x was dispersed in 1 M HCl aqueous solution, other samples were dispersed in neat H_2O.

Table S2. Summary of CONTIN analysis of the DLS correlation traces shown in Figure S9. The main particle population for each sample is indicated in bold.

Sample	Size (nm)	Relative Amount (%)
aCN_x	**3211.9**	**79.8**
	2734500	20.2
bCN_x	282.77	0.6
	1350.9	**88.1**
	138730	11.2
cCN_x	91.171	1.0
	465.87	38.5
	1354.9	**53.3**
	322260	7.2
pCN_x	48.879	0.1
	231.29	6.6
	527.59	22.9
	1651.7	**57.5**
rCNx	**531.82**	**100**
sCNx	131.96	5.3
	656.09	**90.2**
	95872	4.5

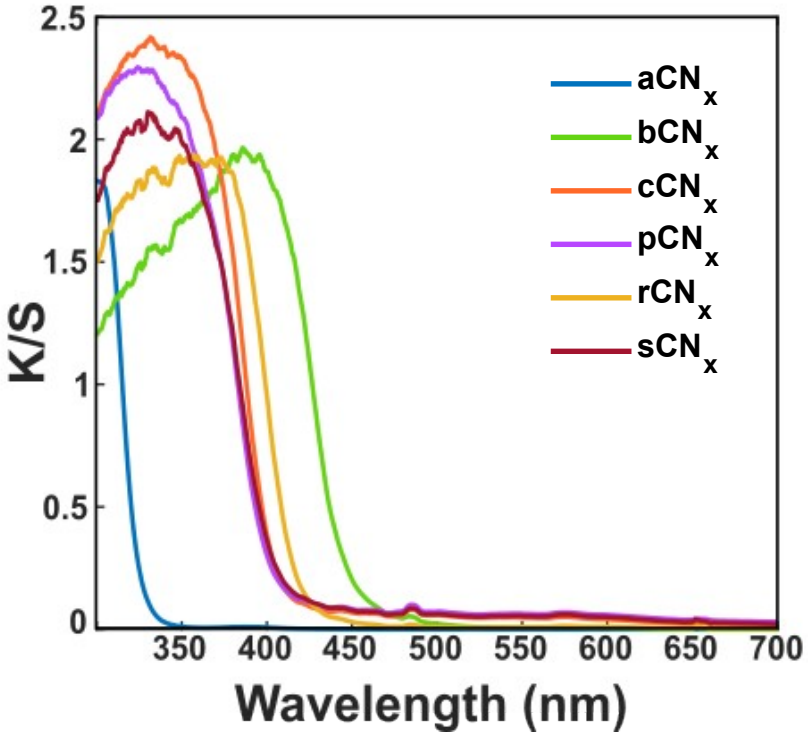

Figure S10. Comparison of the Kubelka-Munk transformed absorbance spectra taken in diffuse reflectance mode of the CN_x samples.

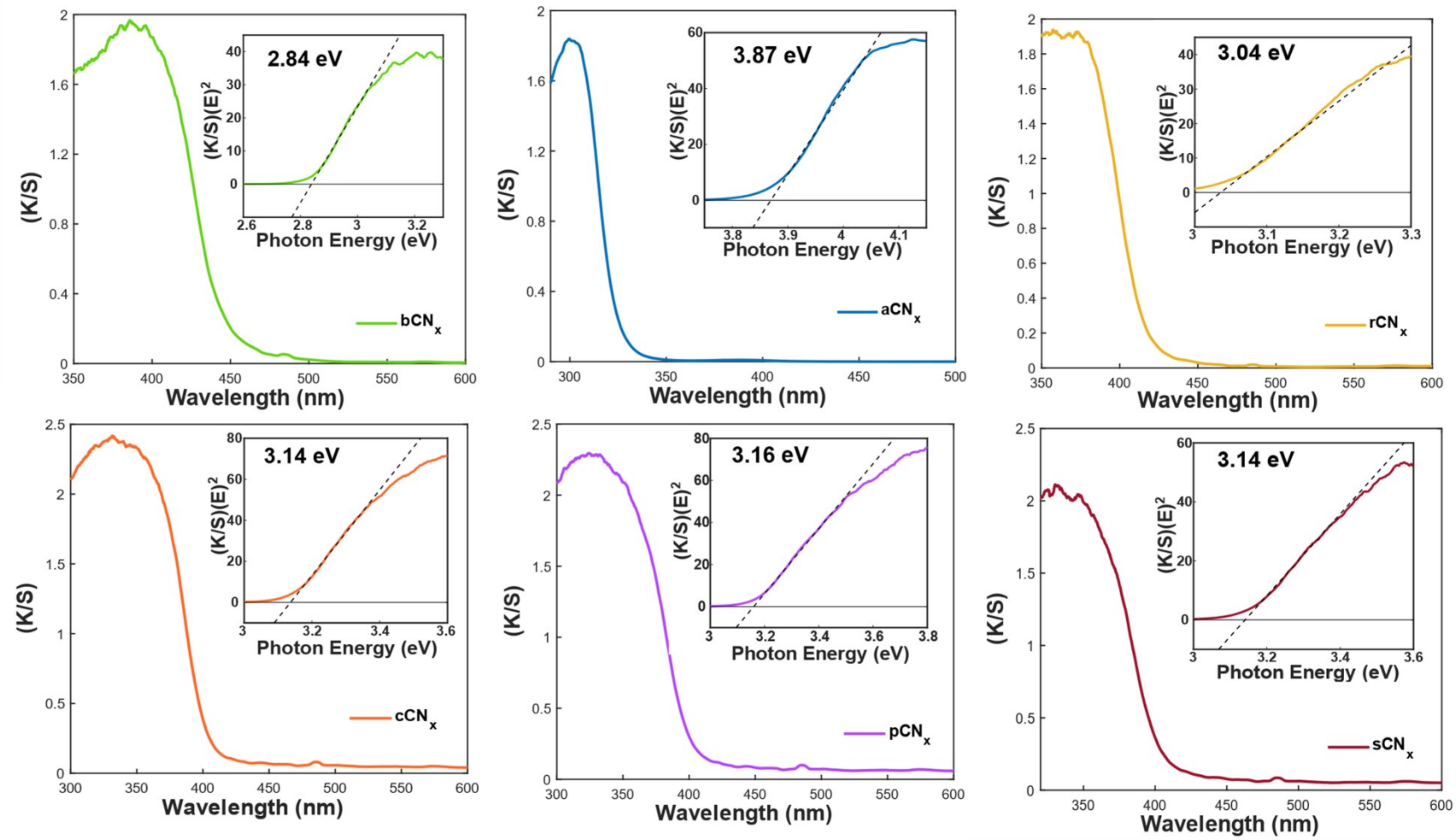

Figure S11. Kubelka-Munk transformed absorbance spectra taken in diffuse reflectance mode of the CN_x samples. The insets show the $(K/S)(E)^2$ vs. photon energy Tauc Plots and their calculated band gap values.

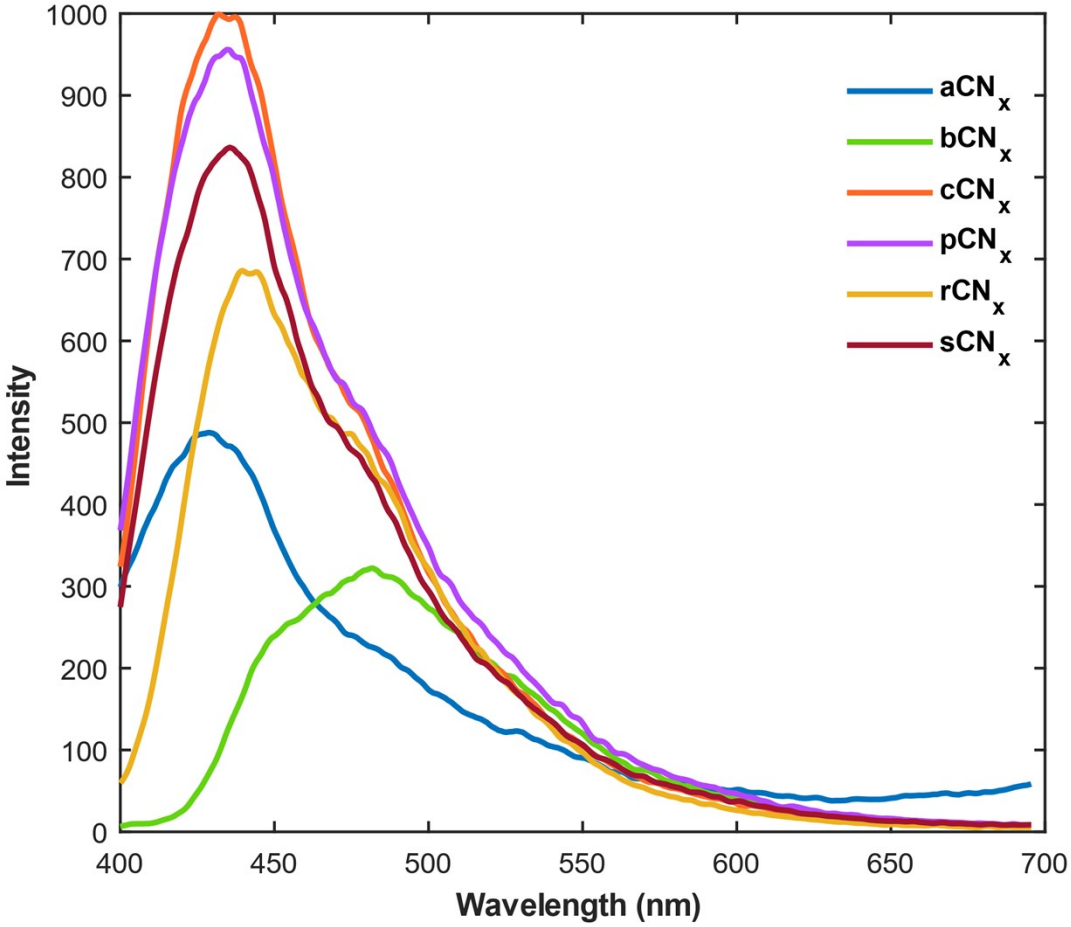

Figure S12. PL spectra of CN_x samples under excitation at 365 nm.

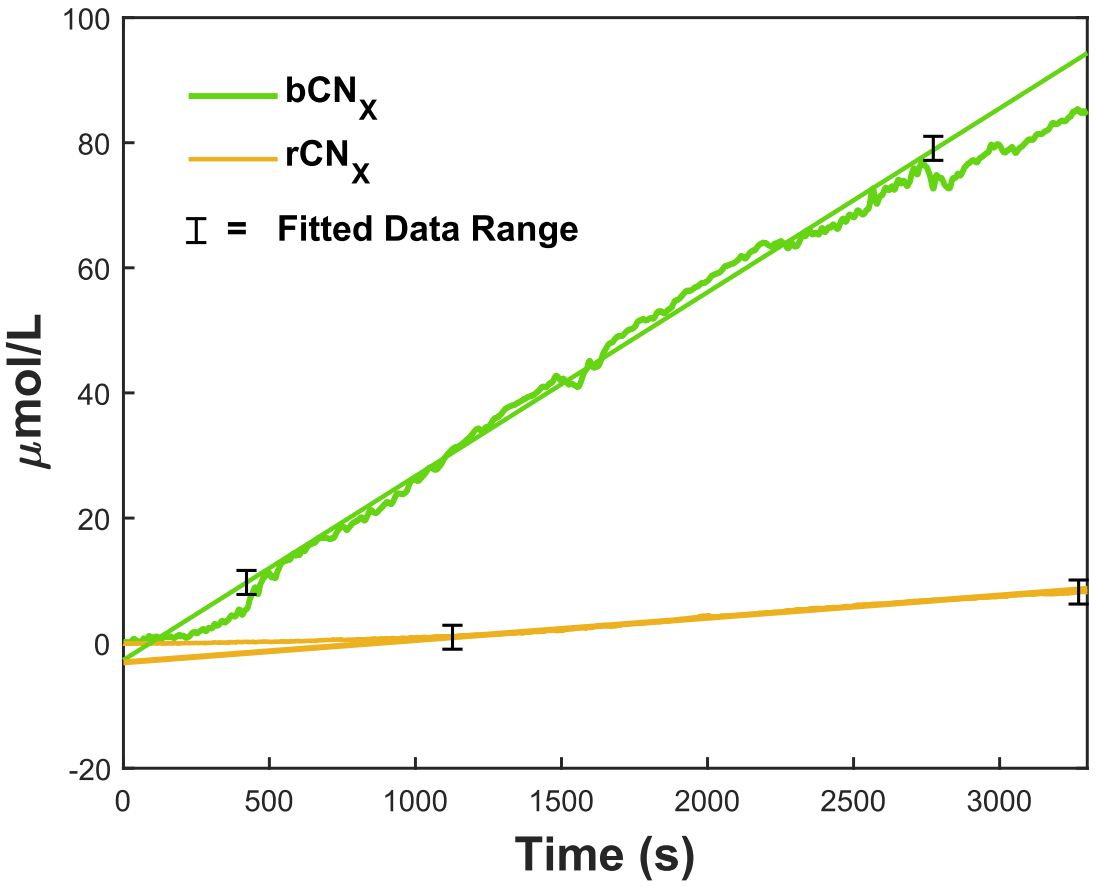

Figure S13. H_2 production over time for bCN_x and rCN_x under excitation with a 405 nm LED.

Table S3. Rates of H_2 production in the HER for samples excited with a 385 nm LED (405 nm LED where indicated).

Semiconductor	Rate 1 (μmols^{-1})	Rate 2 (μmol s^{-1})	Average Rate (μmol s^{-1})	Standard Deviation (μmol s^{-1})
bCN_x - 405 nm	3.5×10^{-4}	4.7×10^{-4}	4.1×10^{-4}	7.9×10^{-5}
rCN_x - 405 nm	3.9×10^{-5}	5.3×10^{-5}	4.6×10^{-5}	9.7×10^{-6}
rCN_x	8.2×10^{-5}	1.08×10^{-4}	9.5×10^{-5}	1.8×10^{-5}
Etched rCN_x	3.29×10^{-4}			
cCN_x	7.3×10^{-5}	8.4×10^{-5}	7.9×10^{-5}	7.9×10^{-6}
pCN_x	5.7×10^{-5}	6.4×10^{-5}	6.0×10^{-5}	5.0×10^{-6}
sCN_x	2.1×10^{-5}	1.93×10^{-5}	1.99×10^{-5}	8.9×10^{-7}

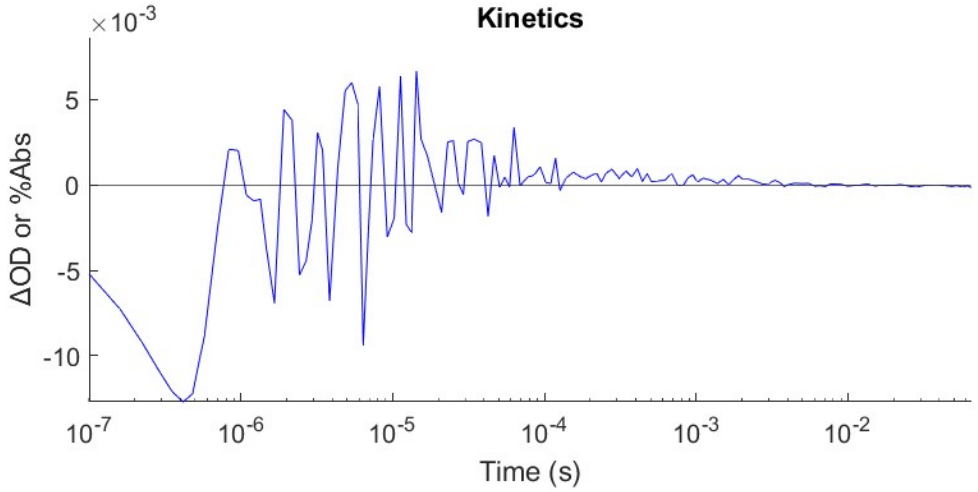

Figure S14. Kinetic trace of aCN_x monitored at 750 nm following excitation at 355 nm.

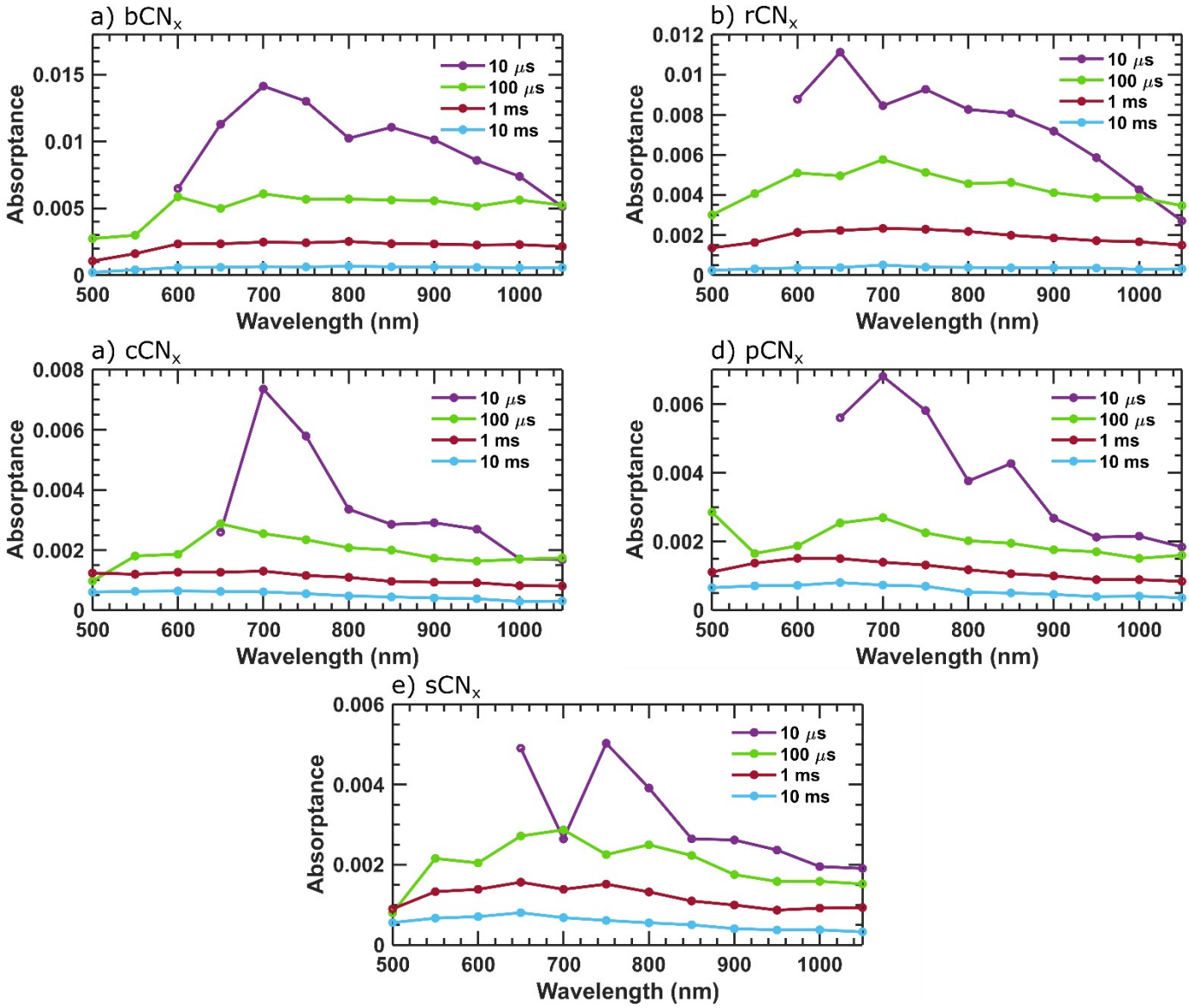

Figure S15. TAS spectra of the CN_x samples following laser excitation at 355 nm at different delay times.

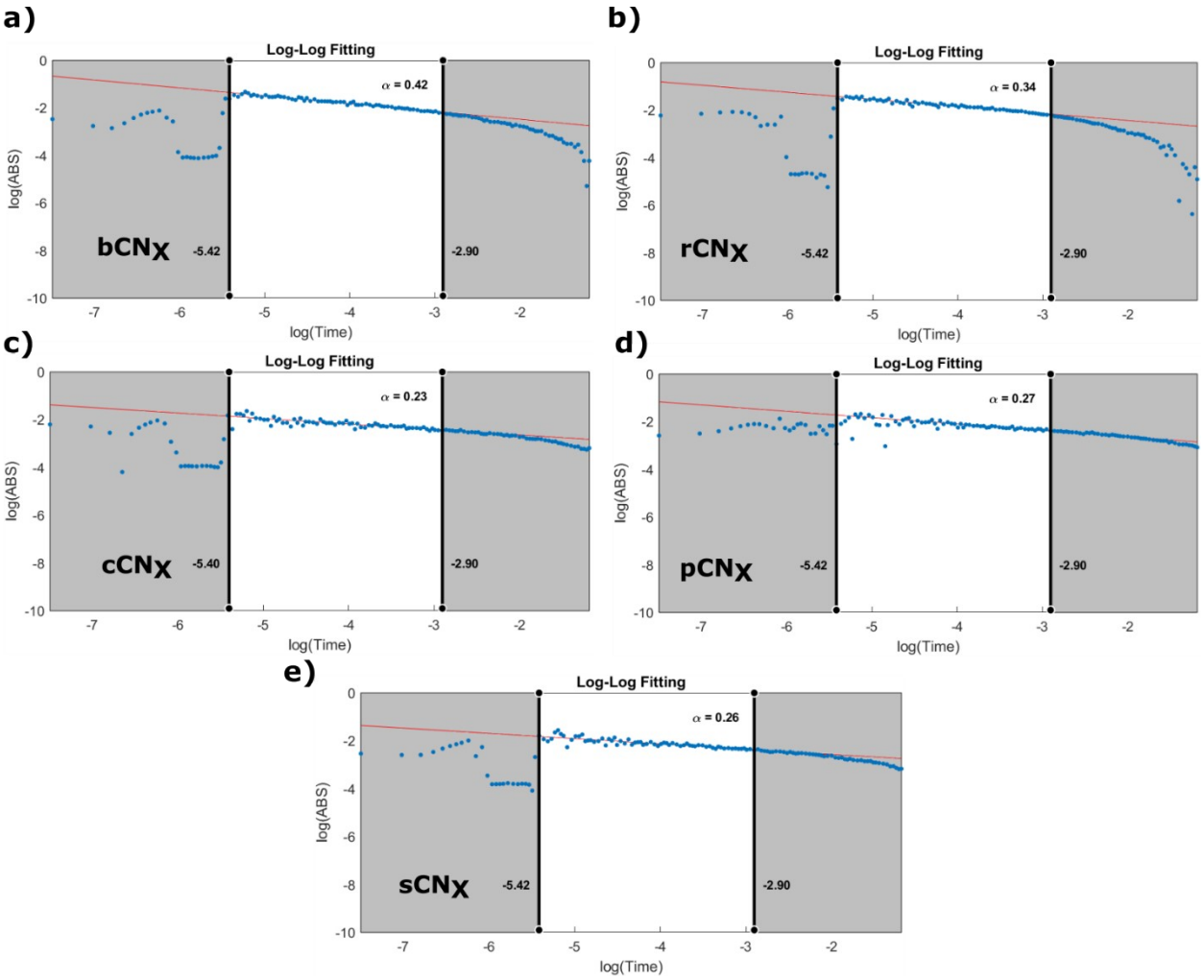

Figure S16. Log(Abs) vs. Log(Time) plots of the decay kinetics at 750 nm following 355 nm laser excitation for the different samples. The data in the gray areas are excluded from the linear fits. The α values represent the negative value of the slopes.

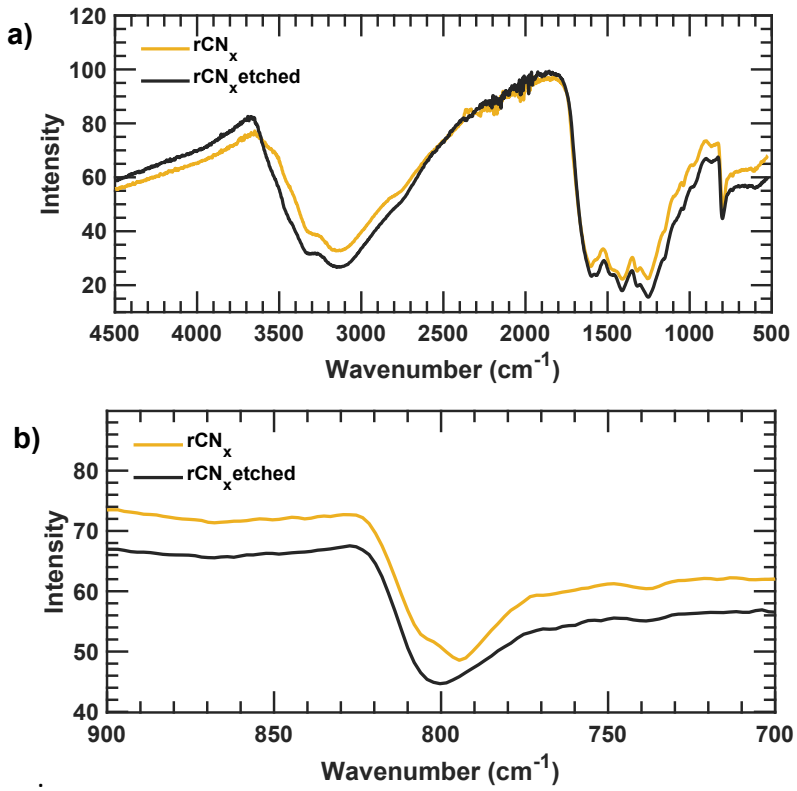

Figure S17. FTIR spectra comparison of rCN_x and rCN_x following the NH_4HF_2 etching treatment. Panel b shows an expanded view of the 900 – 700 cm^{-1} range.

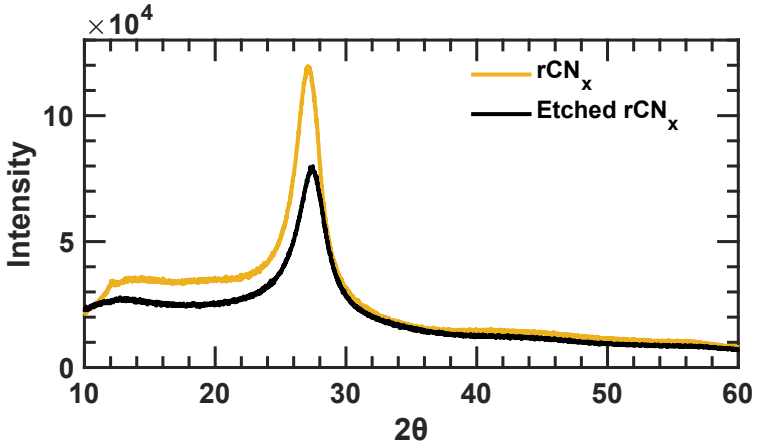

Figure S18. Comparison of the pXRD patterns of rCN_x and rCN_x following the NH_4HF_2 etching treatment. The FWHM of the main peak near 27° is 2.23° before etching and 2.39° after etching.

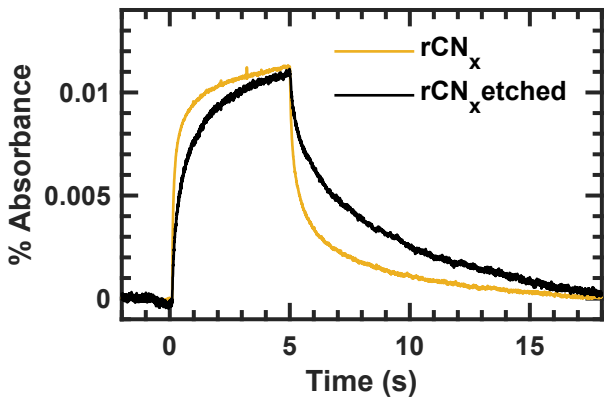

Figure S19. Comparison of the PIAS growth and decays of rCN_x and rCN_x following the NH_4HF_2 etching treatment. 395 nm LED irradiation was started at 0 s and stopped at 5 s.